# Growth Mechanism and Electrical and Magnetic Properties of Ag−Fe$_3$O$_4$ Core−Shell Nanowires

Jingjing Ma,* Kai Wang,* and Maosheng Zhan*

Key Laboratory of Aerospace Advanced Materials and Performance (Ministry of Education), School of Materials Science and Engineering, Beihang University, Beijing 100191, P. R. China

ABSTRACT: One-dimensional Ag−Fe$_3$O$_4$ core−shell hetero-nanowires have been synthesized by a facile and effective coprecipitation method, in which silver nanowires (AgNWs) were used as the nucleation site for growth of Fe$_3$O$_4$ in aqueous solution. The size and morphology control of the core−shell nanowires were achieved by simple adjustments of reaction conditions including FeCl$_3$/FeCl$_2$ concentration, poly(vinylpyrrolidone) (PVP) concentration, reaction temperature, and time. It was found that the Fe$_3$O$_4$ shell thickness could be tuned from 6 to 76 nm with the morphology variation between nanopheres and nanorods. A possible growth mechanism of Ag−Fe$_3$O$_4$ core−shell nanowires was proposed. First, the C=O derived from PVP on the surface of AgNWs provided nucleation points and in situ oxidation reaction between AgNWs and FeCl$_3$/FeCl$_2$ solution promoted the accumulation of Fe^{3+} and Fe^{2+} on the AgNWs surface. Second, Fe$_3$O$_4$ nanoparticles nucleated on the AgNWs surface. Lastly, Fe$_3$O$_4$ nanoparticles grew on the AgNWs surface by using up the reagents. Higher FeCl$_3$/FeCl$_2$ concentration or higher temperature led to faster nucleation and growth, resulting in the formation of Fe$_3$O$_4$ nanorods, whereas lower concentration or lower temperature resulted in slower nucleation and growth, leading to the formation of Fe$_3$O$_4$ nanospheres. Furthermore, the Ag−Fe$_3$O$_4$ core−shell nanowires exhibited good electrical properties and ferromagnetic properties at room temperature. Particularly, the magnetic saturation values (M_s) increased from 5.7 to 26.4 emu g^{-1} with increasing Fe$_3$O$_4$ shell thickness from 9 to 76 nm. This growth of magnetic nanoparticles on 1D metal nanowires is meaningful from both fundamental and applied perspectives.

KEYWORDS: silver nanowires, Fe$_3$O$_4$, core−shell heterostructure, growth mechanism, magnetic property
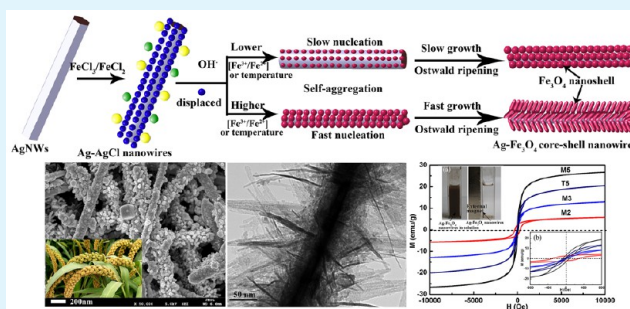
1. INTRODUCTION

One-dimensional (1D) silver nanowires (AgNWs) have attracted considerable attention due to their unique size-dependent optical,[1,2] electrical,[3,4] thermal properties,[5,6] and their various applications in nanoscale electronic devices.[7−9] Particularly, the AgNWs can serve as templates for synthesizing 1D coaxial heterostructured nanowires that can expand their applications because of improved or even novel properties associated with the newly derived nanowires.[10,11] For example, AgNWs have been used as physical templates for the preparation of Ag−SiO$_2$ core−shell nanowires that comprise the AgNWs decorated with uniform SiO$_2$ shells.[12−15] The combination of AgNWs and SiO$_2$ nano-particles in a single composite core−shell heterostructure make the nanowires exhibit an improved fracture resistance and an electron-beam induced shape restoration effect,[13] higher enhancements for surface-enhanced Raman scattering (SERS) applications,[14] and also be used as a kind of effective conductive filler applied in flexible conductive nanocomposites.[15] Afterward, AgNWs were also used as templates for synthesizing Ag−TiO$_2$ core−shell nanowires[16−21] in which thickness of the TiO$_2$ layers could be easily tuned by controlling reaction conditions.[17] These Ag−TiO$_2$ core−shell nanowires exhibit enhanced dye-sensitized solar cells performance[18] and improved photocatalytic activity[19−21] due to their unique multifunctional nanoassembled system.

In addition, AgNWs can also serve as chemical templates to react with FeCl$_3$ for the synthesis of Ag−AgCl core−shell nanowires,[22,23] which displayed enhanced photocatalytic properties. Recently, a novel class of Ag−Cu$_2$O core−shell nanowires[24,25] have been prepared via a facile solution process at room temperature, which showed enhanced photocatalytic activity. It is evident that the fabrication of Ag core−nanomaterial shell heterostructured nanowires has brought new avenues in fundamental nanomaterial research as well as new technological applications. Hence, it is highly desirable to synthesize various Ag−nanomaterials core−shell nanowires.

Recently, Ag core−magnetic nanoparticle shell heterostructured nanowires have attracted much interest because of the combination of unique magnetic and electrical properties. Lin et al.[26] fabricated ordered Ag−nickel core−shell nanowire arrays by electrodeposition, which showed strong magnetic anisotropy with the easily magnetized direction perpendicular to the core−shell nanowires axis. Compared to metal nickel, magnetic Fe$_3$O$_4$-decorated nanostructure materials have attracted more significant and growing amounts of attention due to their various uses

Table 1. Experimental Parameters for the Preparation of All the Samples

samples	raw materials					technology conditions	
	AgNWs, (mM)	FeCl$_3$·6H$_2$O (mM)	FeCl$_2$·4H$_2$O(mM)	PVP (mM)	mass ratio of Fe$_3$O$_4$ to AgNWs[b]	temperature (°C)	reaction time (min)
M1	35	1.6	0.8	7	0.05:1	70	60
M2	35	2.4	1.2	7	0.075:1	70	60
M3[a]	35	4.8	2.4	7	0.15:1	70	60
M4	35	6.4	3.2	7	0.2:1	70	60
M5	35	8.0	4.0	7	0.25:1	70	60
P1	35	4.8	2.4	0	0.15:1	70	60
P2	35	4.8	2.4	3.5	0.15:1	70	60
P3[a]	35	4.8	2.4	7	0.15:1	70	60
P4	35	4.8	2.4	10.5	0.15:1	70	60
P5	35	4.8	2.4	17.5	0.15:1	70	60
T1	35	4.8	2.4	7	0.15:1	40	60
T2	35	4.8	2.4	7	0.15:1	55	60
T3[a]	35	4.8	2.4	7	0.15:1	70	60
T4	35	4.8	2.4	7	0.15:1	85	60
T5	35	4.8	2.4	7	0.15:1	100	60
t1	35	4.8	2.4	7	0.15:1	70	3
t2	35	4.8	2.4	7	0.15:1	70	15
t3	35	4.8	2.4	7	0.15:1	70	30
t4[a]	35	4.8	2.4	7	0.15:1	70	60
t5	35	4.8	2.4	7	0.15:1	70	120
t6	35	4.8	2.4	7	0.15:1	70	240

[a]Determined that experimental parameters were the same. [b]Determined the theoretical yield of Fe$_3$O$_4$ divided by the AgNW mass in the system.

in a range of applications including biomedicine,[27] SERS,[28] wastewater treatment,[29] supercapacitor electrode,[30,31] and microwave absorption.[32–34] If Fe$_3$O$_4$ could be used to coat AgNWs for synthesizing Ag−Fe$_3$O$_4$ core−shell nanowires, the derived nanowires would integrate excellent magnetic and electrical properties to expand their applications. There has been some research on the synthesis and functionality of Ag−Fe$_3$O$_4$ core−shell nanowires. Chen et al.[35] prepared Ag−Fe$_3$O$_4$ core−shell nanowires with a solvent-thermal method in which uniform Fe$_3$O$_4$ shells were bound on the AgNWs. Recently, Li et al.[36] used a facile coprecipitation method to fabricate Ag−Fe$_3$O$_4$ core−shell nanowires which could be highly aligned by an external magnetic field. By contrast, coprecipitation technology overcomes the disadvantages of high reaction temperature, high pressure, time consuming, or the organic solvent use.[37,38] Moreover, the stability of AgNWs under these fabrication conditions is secure.

Nevertheless, no experimental works are available on the growth mechanism of Ag−Fe$_3$O$_4$ core−shell nanowires, which is unfavorable for controlling the resulting structure. What's more, a gap in knowledge remains with regard to the morphological evolutions of Ag−Fe$_3$O$_4$ core−shell nanowires as a function of FeCl$_3$/FeCl$_2$ concentration, poly(vinylpyrolidone) (PVP) concentration, reaction temperature, and reaction time. Moreover, most of the literatures above only focused on one kind of morphology for Fe$_3$O$_4$ coated on the surface of AgNWs, which is unsuitable for the synthesis of core−shell nanowires with different shell morphologies. To the best of our knowledge, there is still no literature reporting a synthesis system that can prepare Ag−Fe$_3$O$_4$ core−shell nanowires with various shell morphologies by simply adjusting the reaction conditions. Thereby, the goal of this paper is to demonstrate the growth mechanism of Fe$_3$O$_4$ on the surface of AgNWs and to obtain stable Ag−Fe$_3$O$_4$ core−shell nanowires with outstanding control over the resulting structure, in which the electrical and magnetic properties can be effectively controlled by the controllable morphology.

Herein, we report a facile coprecipitation route to the mass synthesis of Ag−Fe$_3$O$_4$ core−shell nanowires with different shell morphologies including nanospheres and nanorods in the same synthesis system in the presence of PVP. Detailed and systematic parametric studies on the dependence of morphology of resulting products on the FeCl$_3$/FeCl$_2$ concentration, PVP concentration, temperature, and reaction time were elucidated. Moreover, the in situ oxidation etching between AgNWs and FeCl$_3$/FeCl$_2$ solution is also explored in detail. The results provided insight into the growth mechanism of Ag−Fe$_3$O$_4$ core−shell nanowires. Finally, the magnetic and electrical properties of these Ag−Fe$_3$O$_4$ core−shell nanowires are obtained to determine how particle shape and shell thickness affect their magnetic and electrical characteristics. This growth of magnetic nanoparticles on 1D metal nanowires is meaningful and interesting from both fundamental and applied perspectives.

2. EXPERIMENTAL SECTION

2.1. Materials. AgNO$_3$ (≥99.0% purity), NaCl (≥99.5% purity), FeCl$_3$·6H$_2$O (≥99.0% purity), FeCl$_2$·4H$_2$O (≥99.0% purity), and ethanol were all supplied by Beijing Finechem, China. Ethylene glycol (EG) (≥99.5% purity), NaOH (≥99.5% purity), deionized water, and PVP ($M_w \approx 40000$, ≥ 99.0% purity) were purchased from Xilong Chemical Industry Incorporated Co., Ltd., China. All chemicals were analytical grade and used without further purification.

2.2. Preparation of Ag−Fe$_3$O$_4$ Core−Shell Nanowires. Uniform AgNWs with average diameter of 90 nm and length of 15 μm were synthesized with some modifications by the two-step dropping polyol process, as previously reported by our group.[39,40] Ag−Fe$_3$O$_4$ core−shell nanowires were fabricated by a facile and effective coprecipitation method. In the typical synthesis procedure, 10 mL of 56 mM PVP solution in deionized water was heated to 70 °C until the temperature was steady. Afterward, 30 mL of 90 mM AgNWs solution in deionized water was dropped into the mixture above under N$_2$. Then 20 mL of 19.2 mM FeCl$_3$·6H$_2$O solution in deionized water was added into the flask followed by adding 20 mL of 9.6 mM FeCl$_2$·4H$_2$O solution in deionized water into the mixture. In this case, the Fe^{3+} and Fe^{2+} molar ratio should be 2:1 in order to obtain pure Fe$_3$O$_4$.[33,41] The mixture was
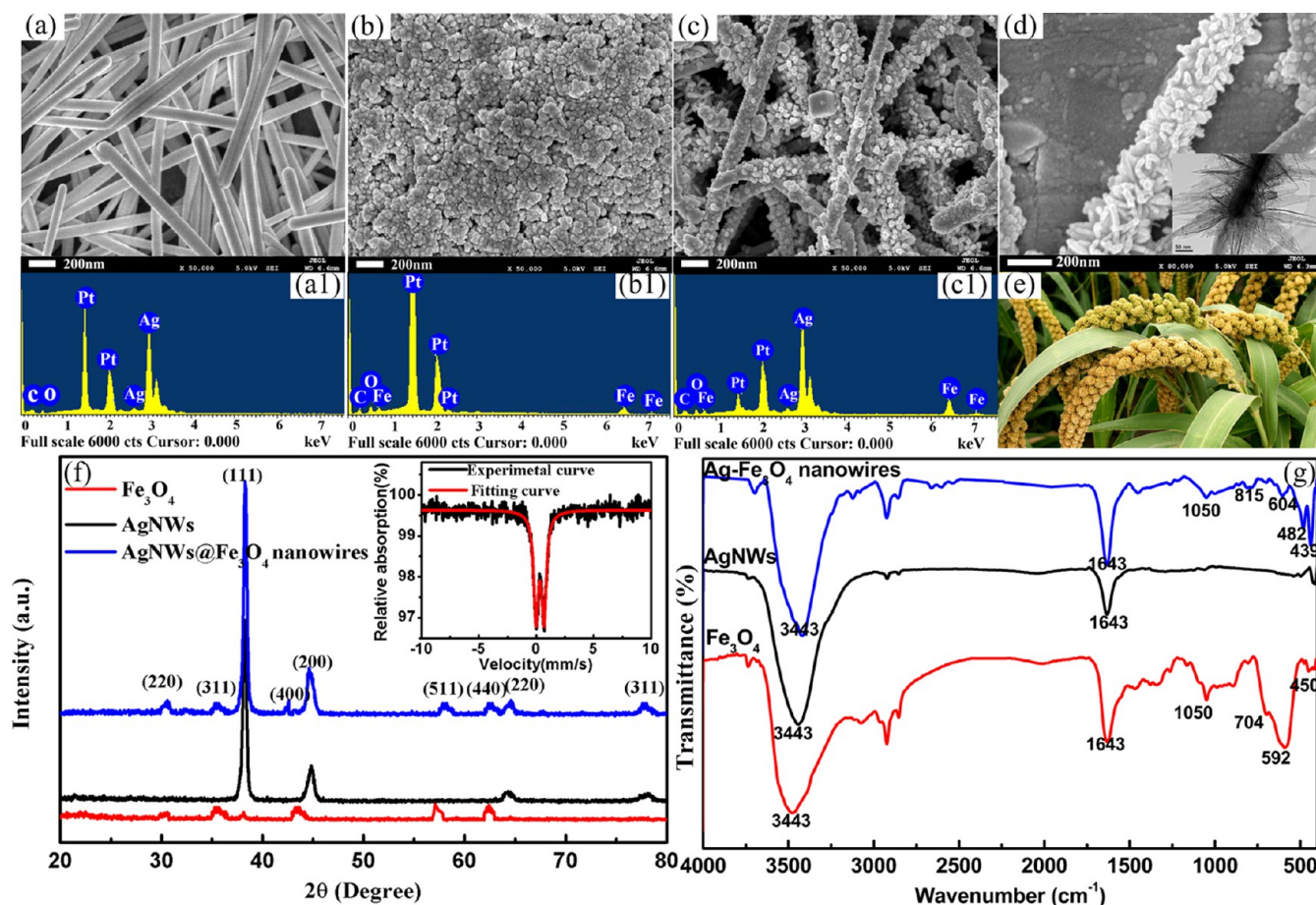
Figure 1. Structural characterization of pure AgNWs, Fe_3O_4, and $Ag-Fe_3O_4$ nanowires: (a) FESEM images of pure AgNWs; (a1) EDX spectrum of pure AgNWs; (b) FESEM images of pure Fe_3O_4; (b1) EDX spectrum of pure Fe_3O_4; (c) FESEM images of $Ag-Fe_3O_4$ core−shell nanowires (sample M5); (c1) EDX spectrum $Ag-Fe_3O_4$ core−shell nanowires; (d) FESEM images of $Ag-Fe_3O_4$ core−shell nanowires at high magnification, and the inset showing its TEM image; (e) structure of icker; (f) XRD patterns, and the inset showing the Mössbauer spectra of $Ag-Fe_3O_4$ nanowires; (g) FTIR spectra.

stirred for 30 min and then a 1 M NaOH solution was injected into the flask until the pH reached 12.[33] The synthesis process was followed by mechanically stirring for 60 min. For those syntheses that produced $Ag-Fe_3O_4$ core−shell nanowires under N_2, the following color changes were noticed: initially silver-white and glistening to yellowish-white, to yellowish-brown, and finally to taupe. The suspension was then washed repeatedly with deionized water and ethanol until pH 7. The final products were dispersed in ethanol and stored at room temperature for further characterization. Pure Fe_3O_4 nanoparticles were also fabricated as the comparative test.

To investigate the effects of the raw materials consisting of $FeCl_3 \cdot 6H_2O/FeCl_2 \cdot 4H_2O$ concentration and PVP concentration, and technological conditions including of temperature and reaction time on the final morphologies of $Ag-Fe_3O_4$ core−shell nanowires, we performed a series of experiments in which the addition of $FeCl_3 \cdot 6H_2O/FeCl_2 \cdot 4H_2O$, the molarity of PVP, temperature, and reaction time were varied from 1.6/0.8 mM to 8.0/4.0 mM (samples M1−M5), from 0.0 to 17.5 mM (samples P1−P5), from 45 to 110 °C (samples T1−T5), and 3 to 240 min (samples t1−t6), respectively. The detailed formulas of these experiments were summarized in Table 1. To further understand the formation mechanism of Fe_3O_4 on the surface of AgNWs, the reaction solutions were extracted at various feeding stages based on the formula of sample M3. They were identified as S1 (AgNWs), S2 (AgNWs/PVP), S3 (AgNWs/PVP/$FeCl_3 \cdot 6H_2O/FeCl_2 \cdot 4H_2O$), S4 (AgNWs/PVP/$FeCl_3 \cdot 6H_2O/FeCl_2 \cdot 4H_2O$/NaOH (pH 8)), and S5 (AgNWs/PVP/$FeCl_3 \cdot 6H_2O/FeCl_2 \cdot 4H_2O$/NaOH (pH 12)), respectively. An experiment in which Fe_3O_4 were synthesized followed by the addition of AgNWs was also carried out.

2.3. Characterization. Field-emission scanning microscopy (FESEM) was carried out with a field-emission scanning electron

microscope (JSM-7500, JEOL) operated at an accelerating voltage of 5 kV and the samples were prepared by drop-casting a drop of the aqueous suspension of samples over a smooth aluminum wafer. The transmission electron microscope (TEM) images were obtained from a JEM-2100 operated at 200 kV and the samples were prepared by placing small droplets of the diluted suspension of samples on copper grids coated with amorphous carbon film. The sizes were determined by individually measuring the diameter of 30 nanostructures by aid of SISAC-IAS image analyzer from the FESEM and TEM images. Results are given as averages with standard deviations. The chemical composites were analyzed with an energy dispersive analyzer (EDX, Oxford Inca). X-ray powder diffraction (XRD) was taken by a D/max 2200 PC X-ray diffractometer operated at a voltage of 40 kV and a current of 40 mA with Cu Kα radiation (λ = 0.15406 nm) at a scanning rate of 0.02°s^{-1} in 2θ ranging from 20° to 80°. FTIR spectra of the samples were obtained using a Nicolet Nexus 670 in which the signal resolution was 1 cm^{-1}. Mössbauer measurements of samples were performed by a digital Mössbauer System MFD-500A with a ^{57}Co (Rh) radioactive source of $\sim 1 \times 10^9$ Bq activity at room temperature. The spectrum evaluation was obtained with the assumption of Lorentzian line shape using Mosswin 3.0i XP software, and the parameters calculated for the spectral components were isomer shift (δ, mm/s) and quadrupole splitting (Δ, mm/s). The surface state of samples was surveyed by X-ray photoelectron spectroscopy (XPS) was performed with an ESCALab 250 electron spectrometer from ThermoFisher Scientific USA using 150 W Al Kα radiation. For the characterization of electrical property, all $I-V$ measurements were tested using a CHID620 Electrochemical Analyzer at room temperature. The measurements were performed under linear sweep mode from −2 to 2 V and the separation between the electrodes was 3 cm. All the samples were prepared by dropping suspension liquid

of nanowires on indium tin oxide (ITO) and dried under vacuum at 50 °C for 6 h. The magnetic properties was recorded on a vibrating sample magnetometer (VSM PPSM-9) at 300 K in ±10 kOe applied field.

3. RESULTS AND DISCUSSION

3.1. Structure Identification of Ag−Fe₃O₄ Core−Shell Nanowires. Figure 1 displays the structural characterization of the pure AgNWs, Fe_3O_4 and Ag−Fe_3O_4 nanowires. From Figure 1a, it could be clearly observed that the neat AgNWs had a relatively smooth surface. From Figure 1b, it was found that the neat Fe_3O_4 clusters synthesized in the absence of AgNWs are of order of 10−30 nm. Notably, large quantities of Ag−Fe_3O_4 heterostructured nanowires with diameter about 143 nm were observed, in which the AgNWs were decorated with Fe_3O_4 nanorods, as shown in Figure 1c. By analyzing the EDX spectrum, we could demonstrate that the heterostructured nanowires mainly consisted of Ag element, Fe element and O element. Figure 1d showed the enlarged image of a single hetro-structured nanowire and inset displayed its TEM image, indicating that their profiles included uniform Fe_3O_4 nanorods shell with thickness of about 76 nm and AgNWs core with diameter of about 61 nm, in which there was a clear layer boundary between them. More interestingly, it seemed that the Ag−Fe_3O_4 core−shell nanowires displayed the structure of icker (Figure 1e). To further demonstrate the crystallinity and phases of the Ag−Fe_3O_4 nanowires, more direct evidence is supplied. Figure 1f showed the XRD patterns of pure Fe_3O_4, AgNWs, and Ag−Fe_3O_4 nanowires. The XRD pattern of the Fe_3O_4 showed peaks at 2θ = 30.1, 35.5, 43.1,57.3, 62.8°, respectively, corresponding to the (220), (311), (400), (511), and (440) refection of Fe_3O_4, which match well with the data from the JCPDS file (no. 75−0033) for cubic Fe_3O_4.[42,43] As for the pattern of AgNWs, diffraction peaks at about 2θ = 38.2, 44.5,64.2, and 77.4° could be perfectively indexed to the (111), (200), (220), and (311) planes of crystal structure for silver (JCPDS File 04−0783).[39] Compared with the pure Fe_3O_4 and AgNWs, the results indicated that the Fe_3O_4−AgNW nanocomposites were a mixture of two phases: AgNWs and Fe_3O_4. Moreover, it is evident that the Fe_3O_4 shell grew on the Ag nanowire core. To further confirm phase purity of Fe_3O_4, we show the Mössbauer spectra of Ag−Fe_3O_4 nanowires in the inset Figure 1f. Only one doublet could be clearly observed in the graph, and no six line spectra appeared. Because the weight percent of AgNWs core was very large and the weight percent of Fe_3O_4 shell was very small in the Ag−Fe_3O_4 nanowires, six line spectra signal was very weak and could not be fitted out. Importantly, the Mössbauer parameters of δ = 0.34 mm/s and Δ = 0.76 mm/s were obtained, which were consistent with the Mössbauer parameters of Fe_3O_4 reported in the previous study.[44,45] The FTIR spectral analysis of pure Fe_3O_4, AgNWs, and the Ag−Fe_3O_4 nanowires are shown in Figure 1g. As for Ag−Fe_3O_4 nanowires, the peaks at 3443, 1643 , 604, and 482 cm^{-1} could be observed. The broad characteristic band in the range of 3443 cm^{-1} can be related to O−H stretching vibrations of the ethanol solvent. The peak at 1645 cm^{-1} should be due to C≡O stretching vibrations of the PVP. The peak at 604 and 482 cm^{-1} are due to the Fe−O stretching mode of the tetrahedral and octahedral sites.[36,46] Notably, by comparing the FT-IR spectrum of pure Fe_3O_4 (592 and 450 cm^{-1}), the stretching vibrations of Fe−O were weakened and red-shifted. These FT-IR spectra provided the useful information that the Fe_3O_4 were successfully bound to the AgNWs.

3.2. Morphological Evolution and Growth Mechanism of Ag−Fe₃O₄ Core−Shell Nanowires. It is well-known that the coprecipitation processing enabled the synthesis of Fe_3O_4
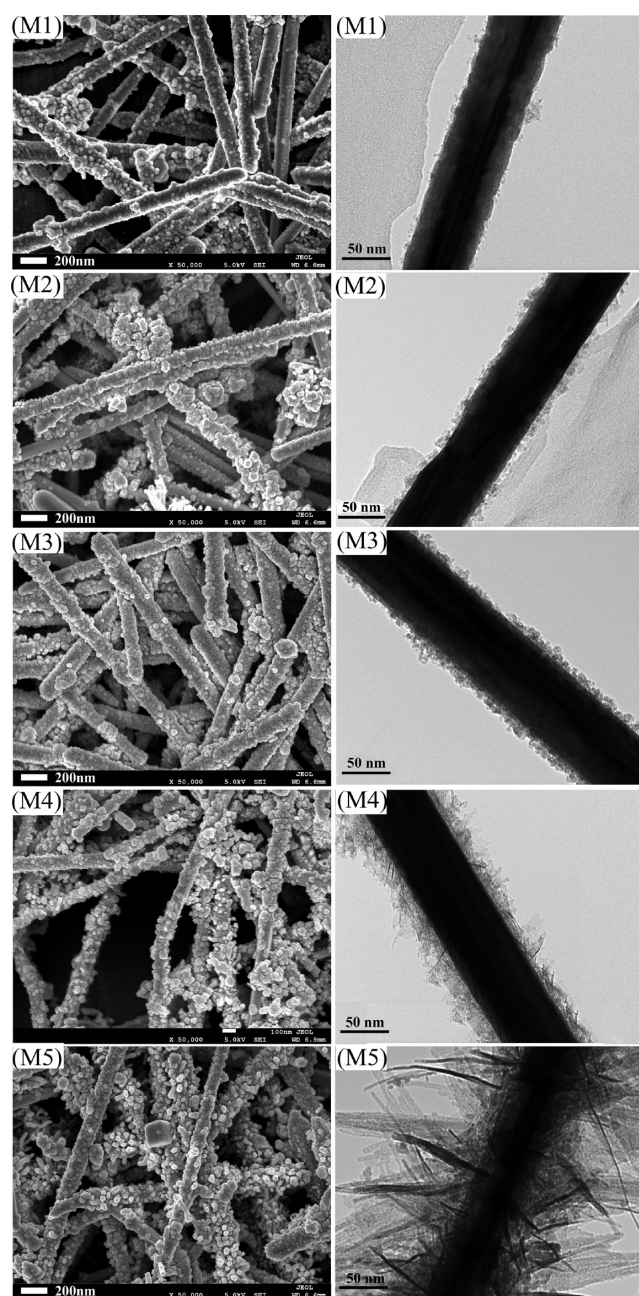
Figure 2. FESEM (left) and TEM (right) images of Ag−Fe_3O_4 core−shell nanowires synthesized with different concentrations of $FeCl_3$·$6H_2O$: (sample M1) 1.6 mM, (sample M2) 2.4 mM, (sample M3) 4.8 mM, (sample M4) 6.4 mM, (sample M5) 8.0 mM.

nanopatricles with different morphologies, depending on the raw materials and technological conditions. In order to understand the formation mechanism of the Ag−Fe_3O_4 core−shell nanowires, we carried out a series of experiments, varying the $FeCl_3$·$6H_2O$/$FeCl_2$·$4H_2O$ concentration, PVP amount, reaction temperature, and reaction time, respectively, and the evidence for which is now shown in detail.

Effects of Raw Materials. 1. Effects of FeCl₃·6H₂O/FeCl₂·4H₂O Concentration. It has been demonstrated that the final morphologies of the shells are strongly dependent on the concentration of the precursor solution.[17,25] In this experiment, we addressed the morphological evolution of the core−shell nanowires with the $FeCl_3$·$6H_2O$/$FeCl_2$·$4H_2O$ concentration.
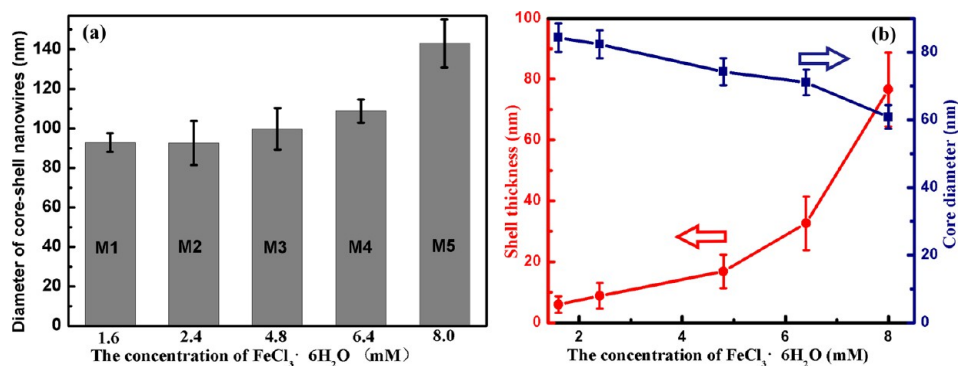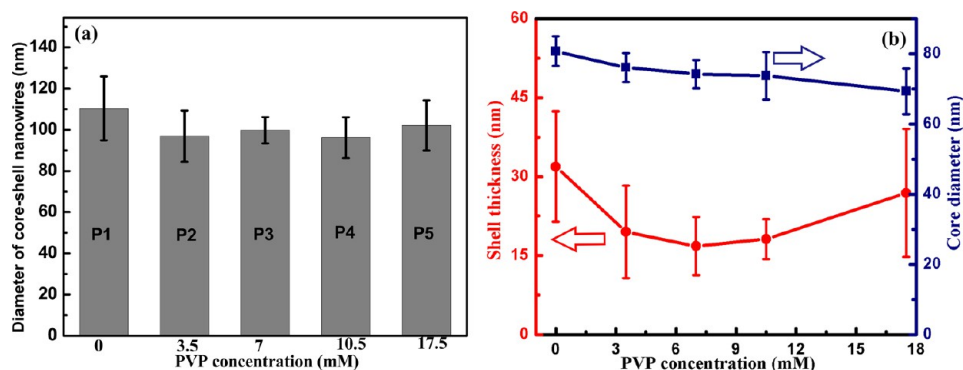
Figure 3. Changes in (a) nanowire diameter and (b) shell thickness and core diameter as a function of the $FeCl_3 \cdot 6H_2O$ concentration.

Because the molar ratio of Fe^{3+} to Fe^{2+} should be 2:1, $FeCl_3 \cdot 6H_2O$ concentration was selected as a representative concentration for simple illustration. FESEM images of the as-synthesized core–shell nanowires with $FeCl_3 \cdot 6H_2O$ concentration of 1.6, 2.4, 4.8, 6.4, and 8.0 mM are displayed in Figure 2 (Left: M1-M5), respectively. Figure 3a shows the changes in nanowire diameter as a function of the $FeCl_3 \cdot 6H_2O$ concentration. It can be clearly observed that Fe_3O_4 nanoparticles are tightly attached on the surface of AgNWs in all images. When $FeCl_3 \cdot 6H_2O$ concentration increased from 1.6 to 8.0 mM, the diameter of core–shell nanowires increased from 90 to 143 nm. To further understand morphology details of the shells and cores for the as-synthesized products, representative TEM images of them are shown in Figure 2 (Right: M1–M5). And Figure 3b shows the changes in core diameter and shell thickness as a function of the $FeCl_3 \cdot 6H_2O$ concentration. It is important to find that the shell thickness increased from 6 to 76 nm, while core diameter decreased from 84 to 60.8 nm with the ferric salt concentration. When the concentration of ferric salt was 1.6 mM, from the FESEM and TEM images of the products (Figure 2 (M1)), incomplete coverage of small Fe_3O_4 nanospheres was obtained. When the $FeCl_3 \cdot 6H_2O$ concentration varied from 1.6 to 4.8 mM, the bigger and denser Fe_3O_4 nanospheres decorated on AgNWs were dominate. Further increasing $FeCl_3 \cdot 6H_2O$ concentration to 6.4 mM leaded to the formation of Fe_3O_4 nanosheets and Fe_3O_4 nanorods besides Fe_3O_4 nanospheres on AgNWs. When the $FeCl_3 \cdot 6H_2O$ concentration was further increased to 8.0 mM, a large amount of icker-like Ag–Fe_3O_4 nanowires appeared, in which Fe_3O_4 nanorods were tightly bound to AgNws. It is well-known that lower concentration of the ferric salt would suppress the nucleation rate of Fe_3O_4 nanoparticles on AgNWs, thereby there was big space between the adjacent Fe_3O_4 nuclei on AgNWs surface. According to the surface-energy minimization, the Fe_3O_4 nuclei would grow along the length of the nanowires,[25] resulting in the formation of the small Fe_3O_4 nanospheres. On the contrary, the higher concentration of the ferric salt leaded to higher nucleation rate and growth rate of Fe_3O_4 nanoparticles. In this case, Fe_3O_4 nucleated simultaneously at many points along the AgNWs. These Fe_3O_4 nuclei began to grow vertically AgNWs surface after their edges touched, leading to rows of Fe_3O_4 nanorods arrays on the surface of AgNWs finally.[25] In addition, nanowires with higher concentration of ferric salt, which led to stronger in situ oxidation reaction between AgNWs and $FeCl_3/FeCl_2$, ended up with smaller cores. Our results indicated that the variation in the ferric salt concentration was effective for controlling the morphology and sizes of core–shell nanowires.

2. Effects of PVP Concentration. It has been demonstrated that the presence of PVP played an important role in the growth of nanocrystals on surface of metal nanowires.[23] FESEM images
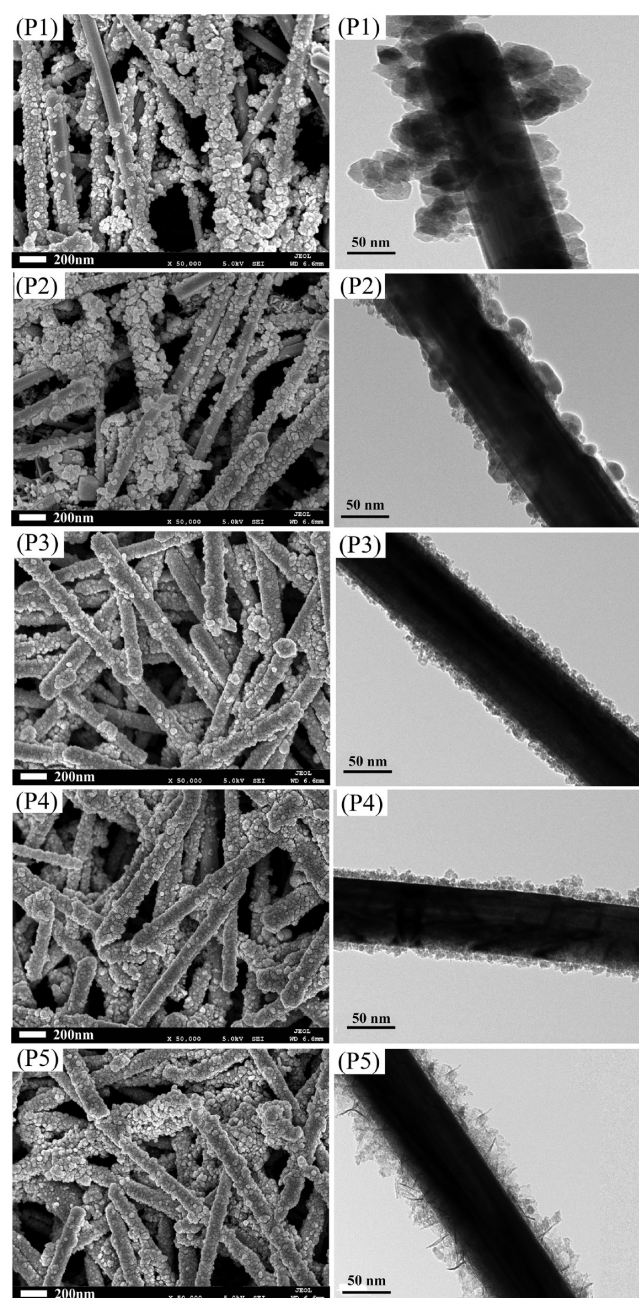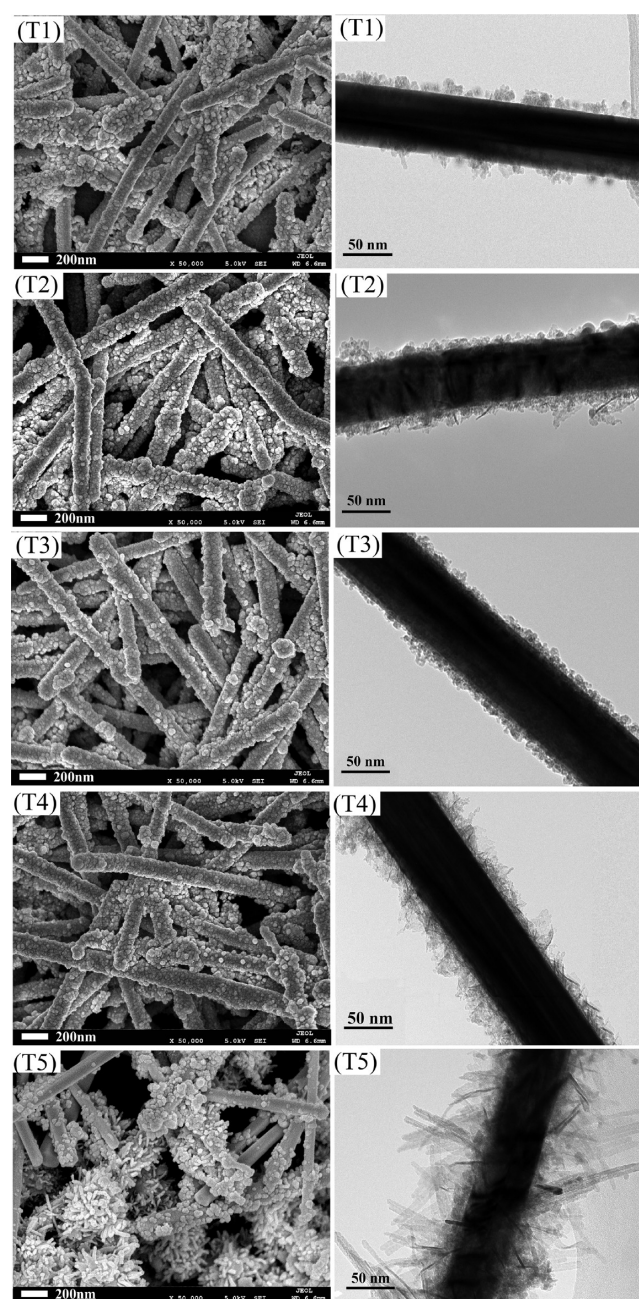

Figure 4. FESEM (left) and TEM (right) images of Ag–Fe_3O_4 core–shell nanowires synthesized with different concentrations of PVP: (sample P1) 0 mM, (sample P2) 3.5 mM, (sample P3) 7 mM, (sample P4) 10.5 mM, (sample P5) 17.5 mM.
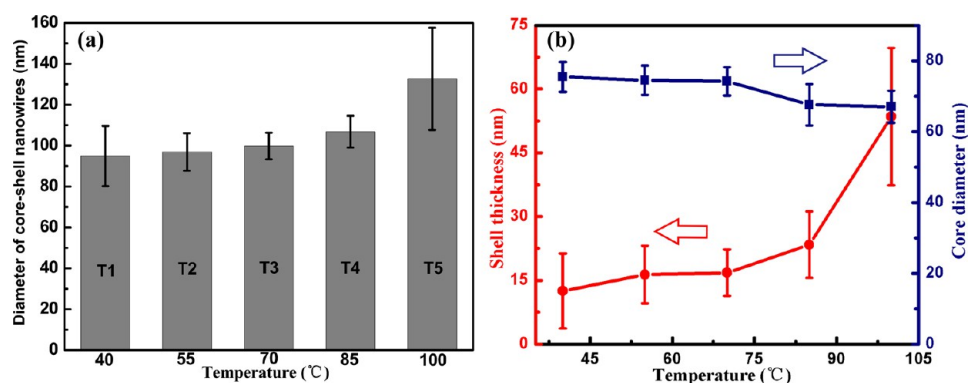
Figure 5. Changes in (a) nanowire diameter and (b) shell thickness and core diameter as a function of the PVP concentration.

of the as-synthesized core−shell nanowires with different PVP amounts of 0, 3.5, 7, 10.5, and 17.5 mM while maintaining the other parameters in the typical process constant, are displayed in Figure 4 (Left: P1−P5), respectively. The effects of PVP concentration on the size and morphology of the core−shell nanowires were further examined by TEM (Figure 4 (Right: P1−P5)). Figure 5 shows the changes in nanowire diameter, core diameter and shell thickness as a function of the PVP concentration. It was found that the nanowires exhibited incomplete shell coverage in which AgNWs had a poor interfacial bonding with the Fe_3O_4 in the absence of PVP, as shown in Figure 4 (P1). Notably, the introduction of PVP improved the interface bonding between AgNWs and Fe_3O_4 and resulted in the formation of Ag−Fe_3O_4 core−shell nanowires with uniform and complete Fe_3O_4 shells. In this case, when the PVP concentration was increased from 3.5 to 17.5 mM, nanowire diameter increased slightly from 97 to 102 nm, correspondingly the shell thickness varied from 19 to 27 nm. Moreover, morphology of Fe_3O_4 decorated on AgNWs surface varied from nanopheres (Figure 4 (P2−P4)) to nanorods with spindle-like tips (Figure 4 (P5)). It has been demonstrated that PVP molecules could be absorbed on the surface of metal nanoparticles through metal-O coordination.[47] In this system, PVP molecules interacted with silver particles through the oxygen atom in carbonyl and were tightly absorbed on the (100) planes of AgNWs according to the surface-energy minimization.[48,49] It is believed that these carbonyl functional groups could provide nucleation points for the formation of metallic oxide.[50] Thus, in the experimental system, there were two possible nucleation sites, i.e., AgNWs substrates and bulk solution, for the growth of Fe_3O_4 nanoparticles. These two sites competed with each other. PVP could be also absorbed on the (100) planes of Fe_3O_4 nuclei, leading to the orientated growth of Fe_3O_4. No PVP or lower concentration of PVP resulted in the higher homogeneous nucleation rate and growth rate in bulk solution. This meant that nanowires, which lacked sufficient ferric salt precursor, ended up with incomplete shell coverage. On the other hand, a higher concentration of PVP resulted in the higher heterogeneous nucleation rate and growth rate on the surface of AgNWs. In this case, Fe_3O_4 nanoparticles grew from the active nucleation centers, and therefore uniform core−shell nanowires with smaller Fe_3O_4 nanopheres were produced finally, possibly due to the particular nucleation promotion and growth suppression of PVP. Particularly, when the PVP concentration increased to a certain extent, due to the extremely strong structure induction effect, a small amount of Fe_3O_4 nanorods with spindle-like tips coated on AgNWs were observed in the system. We speculate that the particular stabilization and structure induction of PVP promote the growth of Fe_3O_4 crystals on the surface of AgNWs and cause the formation of the resultant

Figure 6. FESEM (left) and TEM (right) images of Ag−Fe_3O_4 core−shell nanowires synthesized in different temperature: (sample T1) 40 °C, (sample T2) 55 °C, (sample T3) 70 °C, (sample T4) 85 °C, and (sample T5) 100 °C.

Figure 7. Changes in (a) nanowire diameter and (b) shell thickness and core diameter as a function of the reaction temperature.

Ag−Fe$_3$O$_4$ nanowires with a uniform and perfect core−shell structure.

Effects of Technological Conditions. 1. Effects of Reaction Temperature. It is well-known that temperature is an important factor for morphology-controlling of Fe$_3$O$_4$ nanoparticles.[37,43] Figure 6 (Left: T1−T5) depicts the FESEM images of the products obtained at 40, 55, 70, 85, and 100 °C, respectively, while keeping the other parameters constant. Further insight into the morphology evolution and microstructural details of core−shell nanowires with the temperature were gained by using TEM (Figure 6 (Right: T1−T5)). Changes in nanowire diameter, core diameter, and shell thickness as a function of the temperature are shown in Figure 7. It is important to find that the shell thickness increased from 13 to 53 nm, whereas the core thickness decreased slightly from 78 to 66 nm with the temperature. When the temperature was in the range of 40−55 °C (Figure 6 (T1−T2)), a large amount of agglomerated Fe$_3$O$_4$ nanospheres besides core−shell nanowires were obtained. As the temperature increased to 70 and 85 °C, the uniformity and coverage rate of shells increased and almost no agglomerated Fe$_3$O$_4$ nanospheres were observed at 85 °C (Figure 6 (T3−T4)). Upon the increase in the reaction temperature to 100 °C, a large number of Fe$_3$O$_4$ nanorods with spindle-like tips like flowers begun to form on surface of AgNWs and incomplete shell coverage appeared (Figure 6 (T5)). We speculated that Fe$_3$O$_4$ nuclei on adjacent AgNWs and Fe$_3$O$_4$ nuclei in solution competed for ferric salt precursor. When the temperature was relatively low, the growth rate of Fe$_3$O$_4$ nuclei on AgNWs and Fe$_3$O$_4$ nuclei in solution were at the same level, leading to incomplete shell coverage and agglomerated Fe$_3$O$_4$ nanospheres in solution. As the temperature increased, the faster the molecular movement made the growth rates of Fe$_3$O$_4$ nuclei on AgNWs higher than that of Fe$_3$O$_4$ nuclei in solution, suggesting that nanowires require a larger volume of Fe$_3$O$_4$ nanoparticles for growth. Thus, the Fe$_3$O$_4$ nuclei in solution dissolved into small particles and the Fe$_3$O$_4$ nuclei on the surface of AgNWs grew fast to nanopheres by absorbing these small particles, leading to thicker and uniform shells. When the temperature increased to reflow temperature (100 °C), a large of nuclei edges on the AgNWs surface touched and their growth rate was considerably much higher than that of Fe$_3$O$_4$ nuclei in solution. Moreover, the octahedral Fe$_3$O$_4$ nanoparticles always formed as nucleus and exposed the (111) facet most due to the energetic stability of the (111) facet, which leaded to the 1D growth along the (110) direction.[51] Then adjacent nucleation sites on the AgNWs surface competed for Fe$_3$O$_4$ source, leading to the formation of Fe$_3$O$_4$ nanorods with spindle-like tips like flowers and incomplete shell coverage. Our data indicated that a high temperature is good for

the growth of Fe$_3$O$_4$ nanorods decorated on AgNWs and a low temperature for Fe$_3$O$_4$ nanospheres coated on AgNWs.

2. Effects of Reaction Time. FESEM images of the nanowires synthesized with reaction times of 3, 15, 30, 60, 120, and 240 min, while keeping all the other parameters constant are shown in Figure 8 (Left: t1−t5), respectively. Further insight into the morphology evolution and microstructural details of them with the temperature were gained by using TEM (Figure 8 (Right: t1−t5)). The changes in nanowire diameter, core diameter, and shell thickness with respect to the reaction time are depicted in Figure 9. Uniform core−shell nanowires with diameter of 84.4 nm were dominant products when the reaction time was only 3 min, suggesting that the shell growth was typically fast (3 min for first nucleation and growth stage) (Figure 8 (t1)).When the reaction time was prolonged from 3 to 60 min, the nanowires diameter increased from 84 to 100 nm. In this case, the diameter and the amount of the nanopheres covered on the AgNWs tended to increase (Figure 8 (t2−t3)). Further prolonging the reaction time to 120 and 240 min, the nanowires diameter basically unchanged (Figure 8 (sample t4−t5)). In this case, the Fe$_3$O$_4$ nanoparticles grew by consuming the small particles, and the reduction in surface energy promoted the crystal growth and morphology evolution due to the difference in solubility between larger particles and small particles, according to the Ostwald ripening process.[25,52] Meanwhile, it could be observed that the core diameter kept basically unchanged, suggesting that the oxidation etching of AgNWs by ferric salt have ended after the dropping of NaOH. In this process, with the addition of NaOH, Fe$_3$O$_4$ nanoparticles begun to form on AgNWs surface and Cl$^-$ in the system no longer etched the AgNWs core, leading to the unchanged the core diameter.

Proposed Growth Mechanism of Ag−Fe$_3$O$_4$ Core−Shell Nanowires. To further understand the formation mechanism of Fe$_3$O$_4$ on the surface of AgNWs, the reaction solutions were quenched at various feeding stages based on the formula of sample M3. Figure 10 shows the FESEM images, EDX spectures and TEM images of the structural evolution in this process. As shown in Figure 10 (S1), the surfaces of the pure AgNWs with a pentagonal cross-section were very smooth. When the AgNWs were mixed with PVP solution, the surface of the AgNWs became rougher and the elements C and O proportions increased compared to pure AgNWs (Figure 10 (S2)). We speculated that the PVP molecules were tightly absorbed on the (100) planes of AgNWs. Moreover, TEM image of sample S2 showed that the thickness of PVP layer was about 1−2 nm supporting the phenomenon that PVP were well bound to AgNWs. These carbonyl functional groups on AgNWs would provide nucleation points for the formation of Fe$_3$O$_4$.When the ferric salt aqueous solution
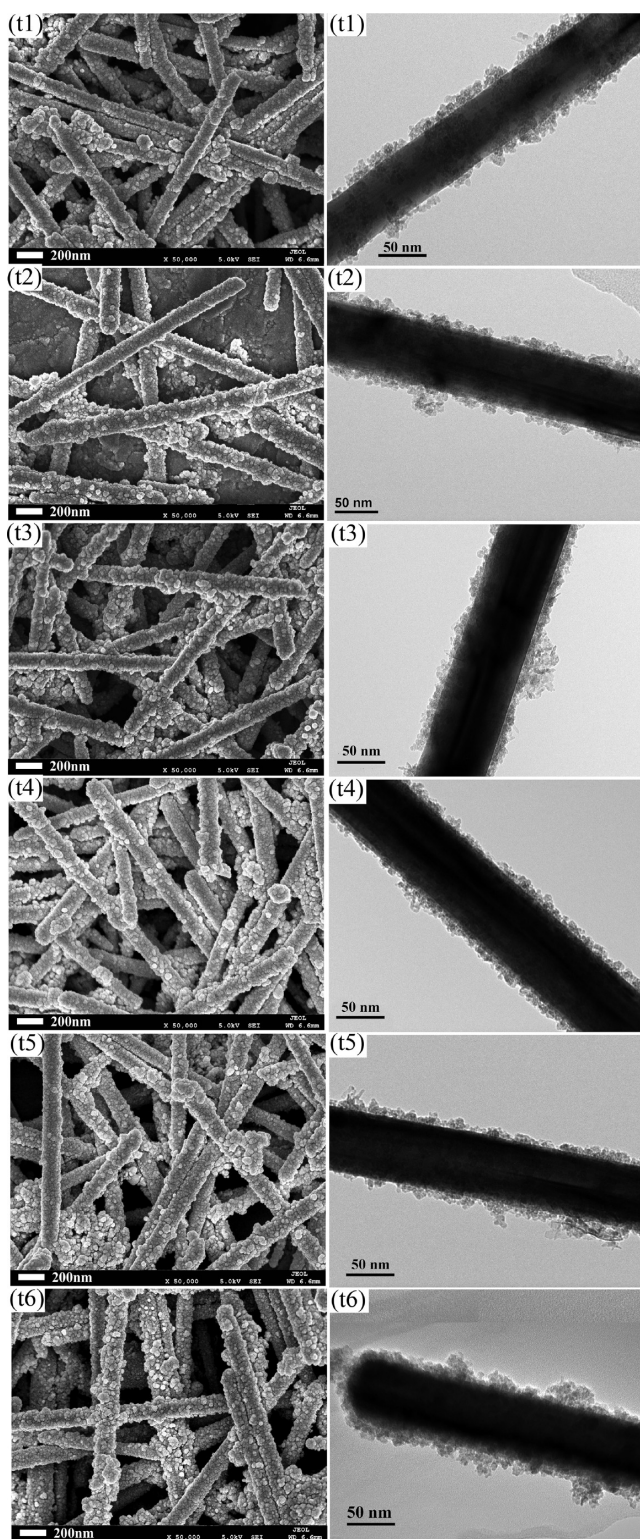
Figure 8. FESEM (left) and TEM (right) images of Ag–Fe₃O₄ core–shell nanowires synthesized with different reaction times: (sample t1) 3 min, (sample t2)15 min, (sample t3) 30 min, (sample t4) 60 min, (sample t5) 120 min, (sample t6) 240 min.

was added into the solution above, the in situ oxidation reaction occurred. It can be clearly seen that a large amount of nano-crystals were coated on surface of AgNWs to form core–shell nanowires and the thickness of nanoshell was about 3−4 nm (Figure 10 (S3)). By analyzing EDX, we speculated that the

composition of shells was AgCl. In this process, the Cl⁻ ions reduced the redox potential of Ag species from +0.80 V (Ag+/Ag) to +0.223 V (AgCl/Ag), thereby Fe^{3+} ions ($E^0_{Fe3+/Fe2+=+0.771 V}$) could oxidize the surface Ag atoms of nanowires into AgCl crystals directly.[23] This would promote the accumulation of Fe^{3+} and Fe^{2+} on the surface of AgNWs. After dropping a small amount of NaOH (pH 8), the surface of AgNWs were coated with a large of small nanoparticals. Further increasing the PH to 12, core−shell nanowires with a uniform structure appeared, correspondingly elements Fe proportion and shell thickness increased. In this process, NaOH reacted with Fe^{2+} and Fe^{3+} absorbed on surface of AgNWs to form Fe_3O_4 nuclei, then Fe_3O_4 shell grew epitaxial on the AgNW core surface. The principle reaction is given as follows

$$2Fe^{3+} + Fe^{2+} + 8OH^- \rightarrow Fe_3O_4 + 4H_2O \qquad (1)$$
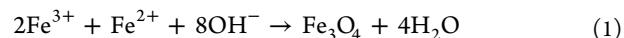
Moreover, AgCl must be displaced during the nucleation of Fe_3O_4, as no interlayer was observed in Figure 10 (S4, S5).

To further clarify the formation mechanism of Fe_3O_4 on the surface of AgNWs, we provide more direct evidence. Figure 11 shows the FTIR spectra of products at different feeding stages based on sample M3. As shown in Figure 11, compared to the spectra of pure AgNWs, the addition of PVP made the absorption bands at 1643 cm⁻¹ assigned to C=O stretching be stronger, demonstrating that PVP was absorbed on AgNWs surface through Ag−O coordination. With the addition of ferric salt aqueous solution, absorption bands at 800 cm⁻¹ assigned to Ag−Cl stretching appeared. Then, when a small amount NaOH was added into the system, the absorption bands at 610 and 502 cm⁻¹ belong to the Fe−O stretching of Fe_3O_4 appeared.[36,46,53] When further increasing the NaOH amount, these absorption bands shifted to 592 and 492 cm⁻¹ and became wider and stronger, demonstrating the growth of Fe_3O_4 shell on AgNWs surface. During this process, the bands at 1643 cm⁻¹ corresponding to the C=O of PVP from sample S3, S4, and S5 still remained, suggesting that the products all contained PVP which was absorbed on AgNWs surface and provided the nucleation points for the formation of Fe_3O_4. However, they seem not change much compared with pure AgNWs. Generally, it is undesirable to make comparisons about characteristic peak intensity of IR between materials with different material composition. In this case, with the formation of AgCl (sample S3) and Fe_3O_4 (sample S5) on AgNWs, the chemical environments of the C=O and the material composition changed. Therefore, we should not make comparisons because they are meaningless. The FTIR spectra data are consistent with the FESEM, EDX, and TEM characterization.

To further confirm the formation mechanism of Ag−Fe_3O_4 core−shell nanowires, we performed XPS spectra of sample S3 and S5. As indicated in Figure 12a, the O 1s peak for sample S3 was observed at 531.9 eV attributed to anionic oxygen in carbonyl functional groups,[52,53] confirming that PVP was absorbed on AgNWs surface, whereas, sample S5 exhibited two O 1s peaks located at 531.5 and 530.3 eV, in which the peak at 530.3 eV might be ascribed to the oxygen in Fe_3O_4.[52,53] Figure 12b shows the peaks of Fe 2p$_{1/2}$ and Fe 2p$_{3/2}$ located at 710.9 and 724.4 eV for sample S5, related to the electron peaks for Fe 2p in Fe_3O_4.[54,55] No shakeup satellite peaks related to the fingerprints of electronic structures of iron oxides like γ-Fe_2O_3 could be identified.[55,56] The Fe 2p$_{1/2}$ and Fe 2p$_{3/2}$ could be resolved using the XPS peak fitting program. Peaks corresponding to 709.6 and 723.1 eV are attributed to +2 oxidation states, whereas 711.2 and 724.6 eV are ascribed to +3 states of iron.[56] Accordingly, the fitting results imply that that relative areas of Fe^{2+} and Fe^{3+} were calculated with the values of 0.337:0.663 for Fe 2p$_{1/2}$ and 0.341:0.659 for Fe 2p$_{3/2}$, respectively,
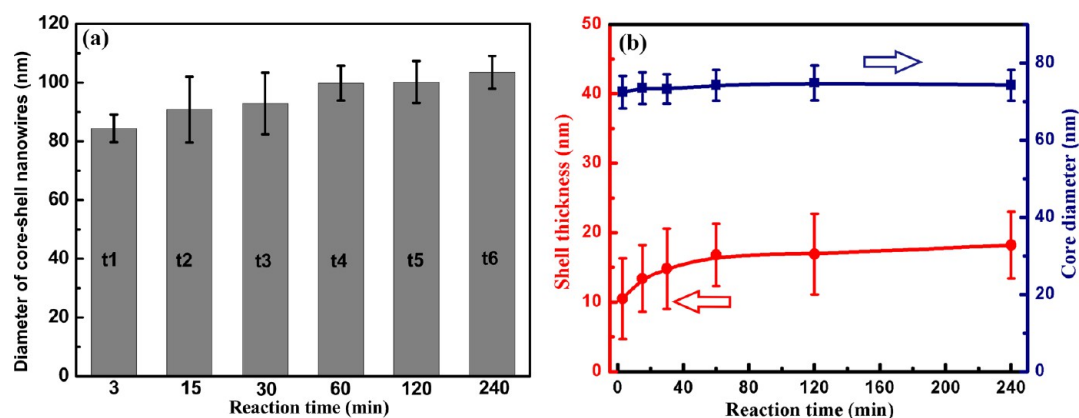
Figure 9. Changes in (a) nanowire diameter and (b) shell thickness and core diameter as a function of the reaction time.
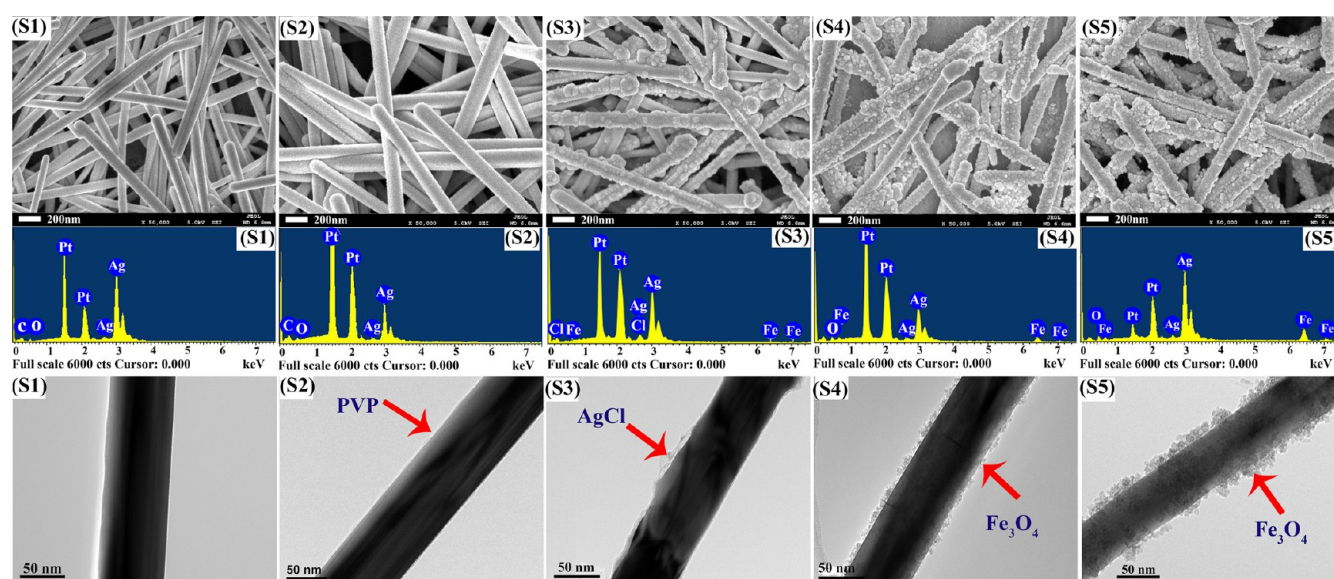

Figure 10. FESEM images (the first row), EDX spectrum (the second row), and TEM images (the third row) of products at different feeding stages for sample M3: (sample S1) AgNWs; (sample S2) AgNWs/PVP; (sample S3) AgNWs/PVP/FeCl$_3$·6H$_2$O/FeCl$_2$·4H$_2$O; (sample S4) AgNWs/PVP/FeCl$_3$·6H$_2$O/FeCl$_2$·4H$_2$O/NaOH (pH 8); (sample S5) AgNWs/PVP/FeCl$_3$·6H$_2$O/FeCl$_2$·4H$_2$O/NaOH (pH 12).
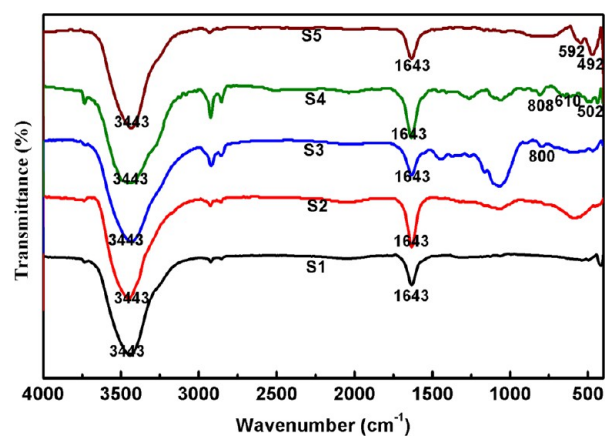

Figure 11. FTIR spectra of products at different feeding stages based on sample M3: (sample S1) AgNWs; (sample S2) AgNWs/PVP; (sample S3) AgNWs/PVP/FeCl$_3$·6H$_2$O/FeCl$_2$·4H$_2$O; (sample S4) AgNWs/PVP/FeCl$_3$·6H$_2$O/FeCl$_2$·4H$_2$O/NaOH (pH 8); (sample S5) AgNWs/PVP/FeCl$_3$·6H$_2$O/FeCl$_2$·4H$_2$O/NaOH (pH 12).

almost corresponding to their molar ratio (1:2) in Fe$_3$O$_4$, which could also be displayed as FeO·Fe$_2$O$_3$. Our XPS data are in good agreement with the Fe 2p spectrum for Fe$_3$O$_4$ reported in the previous study.[50,54,55] The results indicated that the carbonyl functional groups in PVP on AgNWs surface provided nucleation points and Fe$_3$O$_4$ nanoparticles grew on AgNWs. And XPS spectrum of the Fe 2p confirmed the purity of Fe$_3$O$_4$ nanoparticles on AgNWs by the assessment of molar ratio of Fe^{2+} and Fe^{3+}. As shown in Figure 12c, d, the spectrum of Ag 3d$_{3/2}$ and Ag 3d$_{5/2}$ regions for sample S3 are observed at 367.6 and 373.6 eV, respectively.[53] And its Cl 2p$_{2/3}$ peaks are located at 197.4 and 198.8 eV, which were attributed to chlorine in AgCl and chlorine in FeCl$_3$·6H$_2$O or FeCl$_2$·4H$_2$O, respectively. With the addition of NaOH, the Ag 3d spectrum shifted to higher binding energies and their intensity became weaker for sample S5, indicating the formation of shells on the AgNWs, whereas the Cl 2p$_{2/3}$ peaks vanished, suggesting the displacement of AgCl at growth process of Fe$_3$O$_4$ nanoparticles.

Specially, we speculated that the mechanism of Fe$_3$O$_4$ nanoparticles formation in solution followed by adsorption to
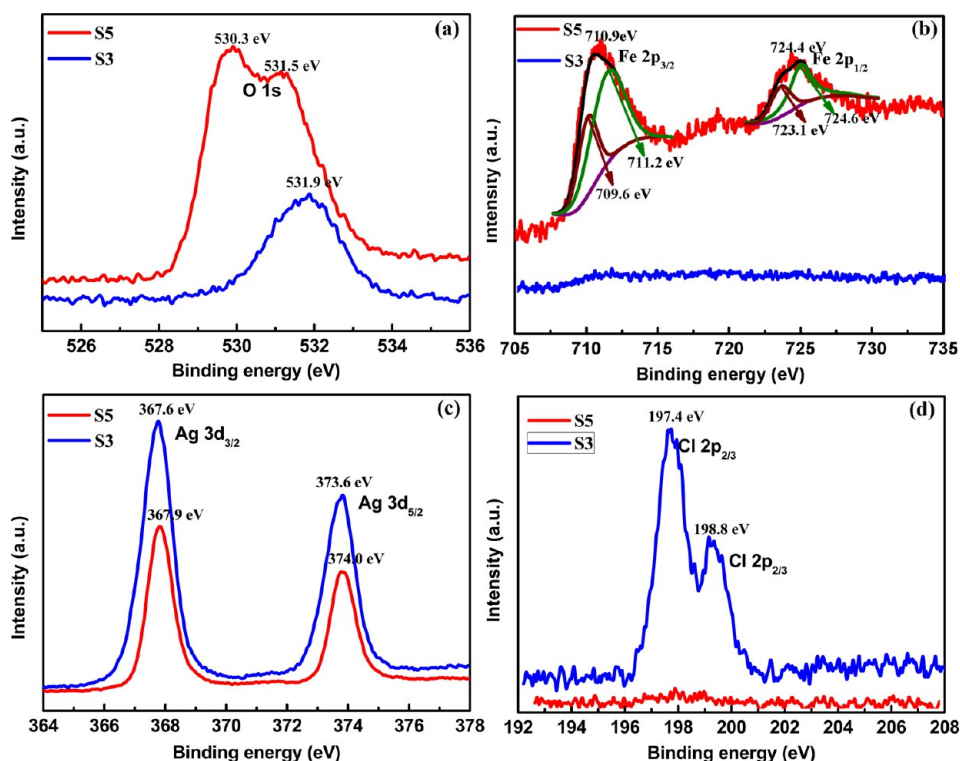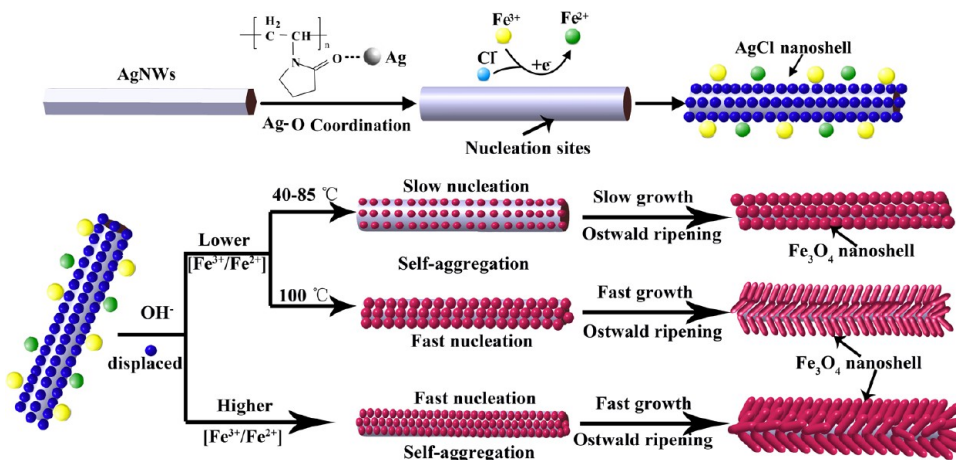
Figure 12. XPS spectra of sample S3 and S5: (a) O 1s spectrum, (b) Fe 2p spectrum, (c) Ag 3d spectrum, (d) Cl 2p spectrum.

Scheme 1. Proposed Scheme of in Situ Growth Mechanism of the Fe$_3$O$_4$ Nanoparticles on the AgNWs Surface by Co-precipitation Method

the AgNWs surface might exist. In order to further confirm this possible mechanism, we carried out an additional experiment in which Fe$_3$O$_4$ nanoparticles were synthesized followed by the addition of AgNWs. It can be seen that only a minute amount of nanoparticles coated on the AgNWs surface. The data indicated that a combined behavior of surface and bulk particle formation in the Ag–Fe$_3$O$_4$ formation mechanism existed, and surface formation was the dominant formation mechanism.

On the basis our experimental results, we proposed that the main formation process of Fe$_3$O$_4$ nanoparticles on the AgNWs surface occurred in three steps: (1) Ag-AgCl core–shell nanowires formation, (2) nucleation of Fe$_3$O$_4$ nanoparticles on the AgNWs surface, (3) Fe$_3$O$_4$ nanoparticles growth until the reagents are used up. The evolution process was illustrated in Scheme 1.

At the first stage, Cl$^-$ ions reduce the redox potential of Ag species markedly from +0.80 V (Ag+/Ag vs SHE) to +0.223 V (AgCl/Ag), inducing the electrons on the surface of the AgNWs. Thereby, Ag atoms on AgNWs surface had been in situ oxidized into AgCl nanocrystals, and Fe^{3+}/ Fe^{2+} couple gathered on AgNWs surface. In addition, the carbonyl functional groups derived from PVP could provide nucleation points for the formation of Fe$_3$O$_4$ nanoparticles. With the introduction of OH$^-$ ions, Fe$_3$O$_4$ nucleates simultaneously at many points along the AgNWs. These Fe$_3$O$_4$ nuclei grow until their edges touch, resulting in rows of perfectly aligned Fe$_3$O$_4$ nanoparticles along AgNWs surface. In this process, higher ferric concentration or higher temperature led to the fast nucleation rate and growth rate, resulting in the formation of Fe$_3$O$_4$ nanorods, whereas lower concentration or lower temperature led to slower nucleation rate and growth rate, resulting in the

formation of Fe_3O_4 nanospheres. Finally, as the reaction continued further, the nanoparticles grow by using up the small particles according to the Ostwald ripening process, and larger nanoparticles were finally formed on the AgNWs surface.

3.3. Influence of Shell Thicknesses on the Electrical and Magnetic Properties of Ag–Fe_3O_4 Core–Shell Nanowires.
On the basis of the above experimental results, various Ag–Fe_3O_4 core–shell nanowires with different shell morphology and thickness have been synthesized by varying $FeCl_3 \cdot 6H_2O$/$FeCl_2 \cdot 4H_2O$ concentration, PVP concentration, reaction temperature and reaction time. As the properties of nanostructures are mainly dependent upon size, shape, and homogeny, it is desirable to obtain materials with desired properties and/or functions for a particular application by precisely maneuvering these parameters. In this section, we addressed how particle shape and shell thickness affected magnetic and electrical characteristics of core–shell nanowires

For the characterization of electrical property, all $I–V$ measurements were tested using a CHID620 Electrochemical Analyzer at room temperature. Linear $I–V$ curves of the representative samples (AgNWs, M2, M3, M5, T5, ITO) were obtained using linear sweep voltammetry in CHID 620 Electrochemical Analyzer at room temperature. The results are shown in Figure 13.
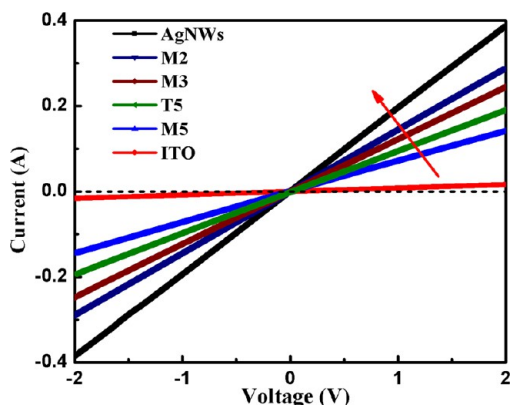
Figure 13. Current–voltage plots of Ag–Fe_3O4 core–shell nanowires with different shell thickness for samples M2, M3, T5, and M5: (sample M2) Fe_3O_4 nanophere shells with thickness of 9 nm; (sample M3) Fe_3O_4 nanophere shells with thickness of 16 nm; (sample T5) Fe_3O_4 nanorod shells with thickness of 54 nm; (sample M5) Fe_3O_4 nanorod shells with thickness of 76 nm.

Compared to the pure AgNWs, the introduction of Fe_3O_4 shell was found to decrease the electrical conductivity (electrical current at the same voltage). Moreover, their electrical conductivity was decreased with increasing Fe_3O_4 shell thickness due to the introduction of the electrically insulating Fe_3O_4 shells. Nevertheless, all core–shell nanowires still exhibited superior electrical properties to ITO, suggesting that Ag–Fe_3O_4 core–shell nanowires can still be used as conductive nanofillers.

The magnetic properties of the representative Ag–Fe_3O_4 core–shell nanowires (samples M2, M3, M5, and T5) with different Fe_3O_4 shell thickness as a function of the applied magnetic field at room temperature are present in Figure 14. The magnetic saturation values (M_s) are 5.7, 12.7, 20.3, and 26.4 emu g^{-1} for sample M2, M3, T5 and M5, respectively, which suggests that the magnetic properties significantly depend on the shell thickness and morphology. Obviously, sample M5 with icker structure possesses the highest magnetic saturation value. In this case, the M_s is about equal to 0.4 times the Ms for pure Fe_3O_4
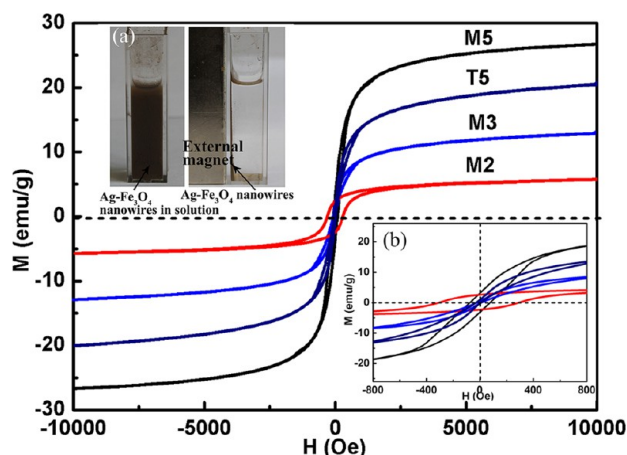
Figure 14. Magnetization curves measured at 300 K of Ag–Fe_3O_4 core–shell nanowires with different shell thickness for samples M2, M3, T5, and M5: (sample M2) Fe_3O_4 nanophere shells with thickness of 9 nm; (sample M3) Fe_3O_4 nanophere shells with thickness of 16 nm; (sample T5) Fe_3O_4 nanorod shells with thickness of 54 nm; (sample M5) Fe_3O_4 nanorods shells with thickness of 76 nm. Inset in a shows magnetic responsive images of sample M5, inset in b shows the close-up of the origin.

nanoparticles reported (66.24 emu g^{-1}),[57] which is greater than the evaluated mass ratio (= 0.25:1) of Fe_3O_4 to AgNWs in the system. This may be due to the small-size effect:[53,57] Fe_3O_4 nanorods coated on the AgNWs exhibited large specific surface area, leading to an increase in unit cell volume and Fe^{2+} content in the sample. Additionally, the in situ oxidation etching on surface of AgNWs and dissolution of AgCl nanocrystal at growth stage of Fe_3O_4 core–shell nanowires would result in a decrease in the AgNWs content. Inset b presents the close-up of the origin. It can be seen that their remanent magnetizations are 2.8, 0.6, 0.9, and 3.2 emu g^{-1}, respectively, indicating that the core–shell nanowires display ferromagnetic behavior. Taking into account the magnetic separation application of core–shell nanowires, sample M5 was selective to be checked its magnetic response in the external applied magnetic field with a magnet and the results was shown in inset Figure 14a. It can be found that Ag–Fe_3O_4 core–shell nanowires dispersed in ethanol can gather for about 40 s in the presence of magnet without residues left in solution state.

4. CONCLUSIONS

It can be demonstrated that under the appropriate experimental conditions, AgNWs can be used as a nucleation site for the growth of pure phase Fe_3O_4 shells in a water environment. By tuning the synthetic parameters, various core diameters and shell thicknesses can be obtained, leading to fine control over electrical and magnetic properties. On the basis of the experimental results, the following conclusions can be drawn:

(1). The result of a formation mechanism investigation revealed that $FeCl_3 \cdot 6H_2O$/$FeCl_2 \cdot 4H_2O$ concentration, PVP concentration, reaction temperature, and time made significant contributions to Fe_3O_4 nanoparticles growth on the surface of AgNWs. Carbonyl functional groups on the AgNWs surface derived from PVP provided nucleation points for the formation of Fe_3O_4. In the first step, the AgNWs were oxidized with $FeCl_3$/$FeCl_2$ solution followed by electrons generated on the AgNWs surface, resulting in the accumulation of Fe^{3+}/Fe^{2+} on the surface of AgNWs.

Then, Fe_3O_4 nanoparticles nucleated on the AgNWs surface and grew by using up the reagents. Moreover, at higher $FeCl_3 \cdot 6H_2O/FeCl_2 \cdot 4H_2O$ or higher temperature, a large amount of Fe_3O_4 nuclei touched and grew vertically on the AgNW surface, leading to rows of Fe_3O_4 nanorod arrays on the surface of AgNWs because of faster nucleation and growth, whereas at lower concentration or lower temperature, a small amount of Fe_3O_4 nuclei did not touch and grew along the AgNWs surface, resulting in the formation of Fe_3O_4 nanospheres coated on AgNWs due to slower nucleation and growth.

(2). The as-synthesized $Ag–Fe_3O_4$ core–shell nanowires exhibited superior electrical properties to ITO at room temperature. And their electrical properties decreased with the increment of the shell thickness because of the introduction of electrically insulating of Fe_3O_4 shells.

(3). The as-synthesized $Ag–Fe_3O_4$ core–shell nanowires exhibited ferromagnetic properties at room temperature, in which the magnetic saturation values (M_s) increased from 5.7 to 26.4 emu g^{-1} with increasing thickness of Fe_3O_4 shell from 9 to 76 nm because of the ferromagnetic properties of Fe_3O_4 shells.

The opportunity to achieve high-quality magnetic nanoparticles grown on AgNWs and understand their growth mechanism is indeed compelling to pursue fundamental researches on relevant properties at the nanoscale. Moreover, the as-synthesized $Ag–Fe_3O_4$ core–shell nanowires may be used as a kind of effective conductive filler applied in flexible conductive nanocomposites for high-performance electromagnetic interference shielding because of outstanding electrical and magnetic properties, which will be our future important work.

■ AUTHOR INFORMATION

Corresponding Authors
*E-mail: majingjingbh@126.com. Tel: +86 10 82338557.
*E-mail: wangkai@buaa.edu.cn.
*E-mail: zhanms@buaa.edu.cn.

Author Contributions
The manuscript was written through contributions of all authors. All authors have given approval to the final version of the manuscript.

Notes
The authors declare no competing financial interest.

■ REFERENCES

(1) Chen, M.; Phang, I. Y.; Lee, M. R.; Yang, J. K. W.; Ling, X. Y. Layer-By-Layer Assembly of Ag Nanowires into 3D Woodpile-like Structures to Achieve High Density "Hot Spots" for Surface-Enhanced Raman Scattering. *Langmuir* **2013**, *29*, 7061−7069.

(2) Yang, S. B.; Choi, H. K.; Lee, D. S.; Choi, C. G.; Choi, S. Y.; Kim, I. D. Improved Optical Sintering Efficiency at the Contacts of Silver Nanowires Encapsulated by a Graphene Layer. *Small* **2015**, *11*, 1293−1300.

(3) Sureshkumar, M.; Na, H. Y.; Ahn, K. H.; Lee, S. J. Conductive Nanocomposites Based on Polystyrene Microspheres and Silver Nanowires by Latex Blending. *ACS Appl. Mater. Interfaces* **2015**, *7*, 756−764.

(4) Guo, F.; Azimi, H.; Hou, Y.; Przybilla, T.; Hu, M.; Bronnbauer, C.; Langner, S.; Spiecker, E.; Forberich, K.; Brabec, C. J. High-Performance Semitransparent Perovskite Solar Cells with Solution-Processed Silver Nanowires as Top Electrodes. *Nanoscale* **2015**, *7*, 1642−1649.

(5) Zilberberg, K.; Gasse, F.; Pagui, R.; Polywka, A.; Behrendt, A.; Trost, S.; Heiderhoff, R.; Görrn, P.; Riedl, T. Hybrid Electronics: Highly Robust Indium-Free Transparent Conductive Electrodes Based on Composites of Silver Nanowires and Conductive Metal Oxides. *Adv. Funct. Mater.* **2014**, *24*, 1650−1650.

(6) Li, Y.; Cui, P.; Wang, L. Y.; Lee, H.; Lee, K.; Lee, H. Highly Bendable, Conductive, and Transparent Film by an Enhanced Adhesion of Silver Nanowires. *ACS Appl. Mater. Interfaces* **2013**, *5*, 9155−9160.

(7) Ghosh, D. S.; Chen, T. L.; Mkhitaryan, V.; Pruneri, V. Ultrathin Transparent Conductive Polyimide Foil Embedding Silver Nanowires. *ACS Appl. Mater. Interfaces* **2014**, *6*, 20943−20948.

(8) Liu, R.; Sun, J.; Cao, D.; Zhang, Li.; Liu, J.; Jiang, G. Fabrication of Highly-Specific SERS Substrates by So-precipitation of Functional Nanomaterials During the Self-sedimentation of Silver Nanowires into a Nanoporous Film. *Chem. Commun.* **2015**, *51*, 1309−1312.

(9) Wang, J.; Jiu, J.; Nogi, M.; Sugahara, T.; Nagao, S.; Koga, H.; He, P.; Suganuma, K. A highly Sensitive and Flexible Pressure Sensor with Electrodes and Elastomeric Interlayer Containing Silver Nanowires. *Nanoscale* **2015**, *7*, 2926−2932.

(10) Sun, Y. Silver Nanowires–Unique Templates for Functional Nanostructures. *Nanoscale* **2010**, *2*, 1626−1642.

(11) Zhang, S. Y.; Liu, J. W.; Zhang, C. L.; Yu, S. H. Co-assembled Thin Films of Ag Nanowires and Functional Nanoparticles at the Liquid−Liquid Interface by Shaking. *Nanoscale* **2013**, *5*, 4223−4229.

(12) Yin, Y.; Lu, Y.; Sun, Y.; Xia, Y. Silver Nanowires can be Directly Coated with Amorphous Silica to Generate Well-controlled Coaxial Nanocables of Silver/Silica. *Nano Lett.* **2002**, *2*, 427−430.

(13) Vlassov, S.; Polyakov, B.; Dorogin, L. M.; Vahtrus, M.; Mets, M.; Antsov, M.; Saar, R.; Romanov, A.; Lõhmus, A. E.; Lõhmus, R. Shape Restoration Effect in Ag−SiO$_2$ Core−Shell Nanowires. *Nano Lett.* **2014**, *14*, 5201−5205.

(14) DeVetter, B. M.; Bhargava, R.; Murphy, C. J. Computational Study of the Surface-Enhanced Raman Scattering from Silica-Coated Silver Nanowires. *Photochem. Photobiol.* **2014**, *90*, 415−418.

(15) Wei, Y.; Chen, S.; Li, F.; Liu, K.; Liu, L. Hybrids of Silver Nanowires and Silica Nanoparticles as Morphology Controlled Conductive Filler Applied in Flexible Conductive Nanocomposites. *Composites, Part A* **2015**, *73*, 195−203.

(16) Du, J.; Zhang, J.; Liu, Z.; Han, B.; Jiang, T.; Huang, Y. Controlled Synthesis of Ag/TiO$_2$ Core-Shell Nanowires with Smooth and Bristled Surfaces via a One-step Solution Route. *Langmuir* **2006**, *22*, 1307−1312.

(17) Ramasamy, P.; Seo, D. M.; Kim, S. H.; Kim, J. Effects of TiO$_2$ Shells on Optical and Thermal Properties of Silver Nanowires. *J. Mater. Chem.* **2012**, *22*, 11651−11657.

(18) Dong, H.; Wu, Z.; Lu, F.; Gao, Y.; El-Shafei, A.; Jiao, B.; Ning, S.; Hou, X. Optics−Electrics Highways: Plasmonic Silver Nanowires@TiO$_2$ Core−Shell Nanocomposites for Enhanced Dye-sensitized Solar Cells Performance. *Nano Energy* **2014**, *10*, 181−191.

(19) Cheng, B.; Le, Y.; Yu, J. Preparation and Enhanced Photocatalytic Activity of Ag@TiO$_2$ Core−Shell Nanocomposite Nanowires. *J. Hazard. Mater.* **2010**, *177*, 971−977.

(20) Dong, Q.; Yu, H.; Jiao, Z.; Lu, G.; Bi, Y. New Facile Synthesis of One-dimensional Ag@ TiO$_2$ Anatase Core−Shell Nanowires for Enhanced Photocatalytic Properties. *RSC Adv.* **2014**, *4*, 59114−59117.

(21) Eom, H.; Jung, J. Y.; Shin, Y.; Kim, S.; Choi, J. H.; Lee, E. J.; Jeong, H.; Park, I. Strong Localized Surface Plasmon Resonance Effects of Ag/TiO$_2$ Core−Shell Nanowire Arrays in UV and Visible Light for Photocatalytic Activity. *Nanoscale* **2014**, *6*, 226−234.

(22) Sun, Y. Conversion of Ag Nanowires to AgCl Nanowires Decorated with Au Nanoparticles and Their Photocatalytic Activity. *J. Phys. Chem. C* **2010**, *114*, 2127−2133.

(23) Bi, Y.; Ye, J. In Situ Oxidation Synthesis of Ag/AgCl Core−Shell Nanowires and Their Photocatalytic Properties. *Chem. Commun.* **2009**, 6551−6553.

(24) Xiong, J.; Li, Z.; Chen, J.; Zhang, S.; Wang, L.; Dou, S. Facile Synthesis of Highly Efficient One-dimensional Plasmonic Photocatalysts through Ag@Cu$_2$O Core−Shell Heteronanowires. *ACS Appl. Mater. Interfaces* **2014**, *6*, 15716−15725.

(25) Sciacca, B.; Mann, S. A.; Tichelaar, F. D.; Zandbergen, H. W.; van Huis, M. A.; Garnett, E. C. Solution-phase Epitaxial Growth of Quasi-monocrystalline Cuprous Oxide on Metal Nanowires. *Nano Lett.* **2014**, *14*, 5891−5898.

(26) Lin, S. C.; Chen, S. Y.; Chen, Y. T.; Cheng, S. Y. Electrochemical Fabrication and Magnetic Properties of Highly Ordered Silver−Nickel Core-Shell Nanowires. *J. Alloys Compd.* **2008**, *449*, 232−236.

(27) Bharath, G.; Prabhu, D.; Mangalaraj, D.; Viswanathan, C.; Ponpandian, N. Facile in Situ Growth of Fe_3O_4 Nanoparticles on Hydroxyapatite Nanorods for pH Dependent Adsorption and Controlled Release of Proteins. *RSC Adv.* **2014**, *4*, 50510−50520.

(28) Zhang, X.; Niu, C.; Wang, Y.; Zhou, S.; Liu, J. Gel-limited Synthesis of Dumbbell-like Fe_3O_4−Ag Composite Microspheres and Their SERS Applications. *Nanoscale* **2014**, *6*, 12618−12625.

(29) Yang, H.; Sun, L.; Zhai, J.; Li, H.; Zhao, Y.; Yu, H. In situ Controllable Synthesis of Magnetic Prussian Blue/Graphene Oxide Nanocomposites for Removal of Radioactive Cesium in water. *J. Mater. Chem. A* **2014**, *2*, 326−332.

(30) Chen, Y.; Song, B.; Li, M.; Lu, L.; Xue, J. Fe_3O_4 Nanoparticles Embedded in Uniform Mesoporous Carbon Spheres for Superior High-Rate Battery Applications. *Adv. Funct. Mater.* **2014**, *24*, 319−326.

(31) Zhang, Z.; Wang, F.; An, Q.; Li, W.; Wu, P. Synthesis of Graphene@ Fe_3O_4@ C Core−Shell Nanosheets for High-performance Lithium ion Batteries. *J. Mater. Chem. A* **2015**, *3*, 7036−7043.

(32) Wang, L.; Huang, Y.; Sun, X.; Huang, H.; Liu, P.; Zong, M.; Wang, Y. Synthesis and Microwave Absorption Enhancement of Graphene@ Fe_3O_4@SiO_2@NiO Nanosheet Hierarchical Structures. *Nanoscale* **2014**, *6*, 3157−3164.

(33) Shen, B.; Zhai, W.; Tao, M.; Ling, J.; Zheng, W. Lightweight, Multifunctional Polyetherimide/Graphene@Fe_3O_4 Composite Foams for Shielding of Electromagnetic Pollution. *ACS Appl. Mater. Interfaces* **2013**, *5*, 11383−11391.

(34) Zhang, H.; Zhu, C.; Chen, Y.; Gao, H. Growth of Fe_3O_4 Nanorod Arrays on Graphene Sheets for Application in Electromagnetic Absorption Fields. *ChemPhysChem* **2014**, *15*, 2261−2266.

(35) Chen, J.; Liu, Y.; Zhu, G.; Yuan, A. Ag@ Fe_3O_4 Nanowire: Fabrication, Characterization and Peroxidase-like Activity. *Cryst. Res. Technol.* **2014**, *49*, 309−314.

(36) Li, N.; Huang, G. W.; Shen, X. J.; Xiao, H.; Fu, S. Y. Controllable Fabrication and Magnetic-field Assisted Alignment of Fe_3O_4-coated Ag Nanowires via a Facile Co-precipitation Method. *J. Mater. Chem. C* **2013**, *1*, 4879−4884.

(37) Lim, Y. S.; Lai, C. W.; Hamid, S. B. A.; Julkapli, N. M.W.; Yehya, A.; Karim, M. Z.; Tai, M. F.; Lau, K. S. A study on Growth Formation of Nano-sized Magnetite Fe_3O_4 via Co-precipitation Method. *Mater. Res. Innovations* **2014**, *18*, 457−461.

(38) Wu, S.; Sun, A.; Zhai, F.; Wang, J.; Xu, W.; Zhang, Q.; Volinsky, A. A. Fe_3O_4 Magnetic Nanoparticles Synthesis from Tailings by Ultrasonic Chemical Co-precipitation. *Mater. Lett.* **2011**, *65*, 1882−1884.

(39) Ma, J.; Zhan, M. Rapid Production of Silver Nanowires Based on High Concentration of $AgNO_3$ Precursor and Use of $FeCl_3$ as Reaction Promoter. *RSC Adv.* **2014**, *4*, 21060−21071.

(40) Ma, J.; Zhan, M. S.; Wang, K. Ultra-lightweight Silver Nanowires Hybrid Polyimide Composite Foams for High-Performance Electromagnetic Interference Shielding. *ACS Appl. Mater. Interfaces* **2015**, *7*, 563−576.

(41) Pu, H.; Jiang, F. Towards High Sedimentation Stability: Magnetorheological Fluids Based on CNT/Fe_3O_4 Nanocomposites. *Nanotechnology* **2005**, *16*, 1486−1489.

(42) Baker, A. M.; Wang, L.; Advani, S. G.; Prasad, A. K. Nafion Membranes Reinforced with Magnetically Controlled Fe_3O_4−MWCNTs for PEMFCs. *J. Mater. Chem.* **2012**, *22*, 14008−14012.

(43) Ren, Y.; Zhu, C.; Zhang, S.; Li, C.; Chen, Y.; Gao, P.; Yang, P.; Ouyang, Q. Three-dimensional SiO_2@Fe_3O_4 Core/Shell Nanorod Array/Graphene Architecture: Synthesis and Electromagnetic Absorption properties. *Nanoscale* **2013**, *5*, 12296−12303.

(44) Fang, S.; Liu, Z.; Chen, Y.; Huo, M.; Bian, D.; Yang, X.; Geng, Z.; Zhu, S. Synthesis of Magnetic Materials by Solvothermal Method with Iron-mud and Adsorption of Methylene Blue in Aqueous Solution. *Chin. J. Nonferr. Metal* **2015**, *4*, 1109−1115.

(45) Wu, W. Mossbauer Spectroscopy and Its Application to Analyse of Fe in the Materials. *Mod. Instrum.* **2000**, *5*, 39−43.

(46) Gao, Q.; Zhao, A.; Gan, Z.; Tao, W.; Li, D.; Zhang, M.; Guo, H.; Wang, D.; Sun, H.; Mao, R.; Liu, E. Facile Fabrication and Growth Mechanism of 3D Flower-like Fe_3O_4 Nanostructures and Their Application as SERS Substrates. *CrystEngComm* **2012**, *14*, 4834−4842.

(47) Huang, H. H.; Ni, X. P.; Loy, G. L.; Chew, C. H.; Tan, K. L.; Loh, F. C.; Deng, J. F.; Xu, G. Q. Photochemical Formation of Silver Nanoparticles in Poly(N-vinylpyrrolidone). *Langmuir* **1996**, *12*, 909−912.

(48) Wiley, B.; Sun, Y.; Mayers, B.; Xia, Y. Shape-Controlled Synthesis of Metal Nanostructures: The Case of Silver. *Chem. - Eur. J.* **2005**, *11*, 454−463.

(49) Gao, Y.; Jiang, P.; Liu, D. F.; Yuan, H. J.; Yan, X. Q.; Zhou, Z. P.; Wang, J. X.; Song, L.; Liu, L. F.; Zhou, W. Y.; Wang, G.; Wang, C. Y.; Xie, S. S. Evidence for the Monolayer Assembly of Poly(vinylpyrrolidone) on the Surfaces of Silver Nanowires. *J. Phys. Chem. B* **2004**, *108*, 12877−12881.

(50) Song, W. L.; Guan, X. T.; Fan, L. Z.; Cao, W.; Wang, C.; Zhao, Q.; Cao, M. Magnetic and Conductive Graphene Papers toward Thin Layers of Effective Electromagnetic Shielding. *J. Mater. Chem. A* **2015**, *3*, 2097−2107.

(51) Yang, C.; Wu, J.; Hou, Y. Fe_3O_4 Nanostructures: Synthesis, Growth Mechanism, Properties and Applications. *Chem. Commun.* **2011**, *47*, 5130−5141.

(52) Mu, J.; Chen, B.; Guo, Z.; Zhang, M.; Zhang, Z.; Zhang, P.; Shao, C.; Liu, Y. Highly Dispersed Fe_3O_4 Nanosheets on One-dimensional Carbon Nanofibers: Synthesis, Formation Mechanism, and Electrochemical Performance as Supercapacitor Electrode Materials. *Nanoscale* **2011**, *3*, 5034−5040.

(53) Amarjargal, A.; Tijing, L. D.; Im, I. T.; Kim, C. S. Simultaneous Preparation of Ag/Fe_3O_4 Core−Shell Nanocomposites with Enhanced Magnetic Moment and Strong Antibacterial and Catalytic Properties. *Chem. Eng. J.* **2013**, *226*, 243−254.

(54) Shi, H.; Tan, L.; Du, Q.; Chen, X.; Li, L.; Liu, T.; Fu, C.; Liu, H.; Meng, X. Green Synthesis of Fe_3O_4 Nanoparticles with Controlled Morphologies Using Urease and Their Application in Dye Adsorption. *Dalton T.* **2014**, *43*, 12474−12479.

(55) Ji, L.; Zhou, L.; Bai, X.; Shao, Y.; Zhao, G.; Qu, Y.; Wang, C.; Li, Y. Facile Synthesis of Multiwall Carbon Nanotubes/Iron Oxides for Removal of Tetrabromobisphenol A and Pb (II). *J. Mater. Chem.* **2012**, *22*, 15853−15862.

(56) Pradhan, G. K.; Parida, K. M. Fabrication, Growth mechanism, and Characterization of α-Fe_2O_3 Nanorods. *ACS Appl. Mater. Interfaces* **2011**, *3*, 317−323.

(57) Wu, W.; Xiao, X.; Zhang, S.; Zhou, J.; Fan, L.; Ren, F.; Jiang, C. Large-scale and Controlled Synthesis of Iron Oxide Magnetic Short Nanotubes: Shape Evolution, Growth Mechanism, and Magnetic Properties. *J. Phys. Chem. C* **2010**, *114*, 16092−16103.